# On the Mechanism Responsible of the Varying Adsorption Affinities of $CO_2$, $N_2$ and $H_2O$ on Graphtriyne Membranes

Yusuf Bramastya Apriliyanto[1], Luca Mancini[2], Noelia Faginas-Lago[2], and Marcos Mandado[3](✉)

[1] Department of Chemistry, The Republic of Indonesia Defense University, Kampus Unhan Komplek IPSC Sentul, 16810 Bogor, Indonesia
[2] Department of Chemistry, Biology and Biotechnology, University of Perugia, & UdR INSTM di Perugia, Via Elce di Sotto 8, 06123 Perugia, Italy
[3] Department of Physical Chemistry, University of Vigo, Lagoas-Marcosende s/n, 36310 Vigo, Spain
mandado@uvigo.es

**Abstract.** Deformation Density based Energy Decomposition Analysis (DD-EDA) of the interaction energy between $CO_2$, $N_2$, and $H_2O$ and graphtriyne membranes was performed at the DFT-D3 level to elucidate the energy components responsible for the differences in adsorption affinity. Previous explanations at a qualitative level were based on electric dipole and polarizability scales. Surprisingly, neither electrostatic nor polarization interactions primarily account for $CO_2$'s strongest adsorption affinity to a monolayer membrane. Instead, Pauli repulsion governs the adsorption affinity, with $CO_2$ experiencing the lowest Pauli repulsion energy, not showing the more negative polarization or electrostatic energies. The stability of these three molecules within a trilayer membrane follows the same order as in a monolayer. However, in this case, $CO_2$ exhibits the highest Pauli repulsion energy, which is largely offset by its more negative polarization and electrostatic energies. This variation can be attributed to the distinct trends observed in the energy-versus-distance profiles of these gases with a monolayer membrane. These preliminary results, derived from static simulations, should be further validated against those obtained from dynamic simulations.

**Keywords:** Graphtriyne Membrane · Gas Adsorption · Energy Decomposition Analysis · Density Functional Theory · Computational Chemistry

## 1 Introduction

Membrane technology has gained significant attention as a highly energy-efficient and scalable solution for gas separation and storage, particularly in industries such as hydrogen production, natural gas purification, and carbon capture [1, 3]. Among various membrane materials, carbon-based membranes have emerged as a promising class due to their unique structural properties, high thermal and chemical stability, and tunable selectivity.

© The Author(s), under exclusive license to Springer Nature Switzerland AG 2026
O. Gervasi et al. (Eds.): ICCSA 2025 Workshops, LNCS 15897, pp. 39–52, 2026.
https://doi.org/10.1007/978-3-031-97660-5_4

Over the past few decades, extensive research efforts have been dedicated to optimizing their microstructure, improving separation performance, and enabling large-scale applications [4, 5].

The development of carbon molecular sieve (CMS) membranes marked a pivotal advancement, as these materials demonstrated exceptional size-selective gas transport due to their precisely controlled microporous structures. Further innovations in porous carbon materials, including activated and templated carbons, enhanced gas adsorption capacity and selectivity by tailoring pore architecture. The advent of two-dimensional materials, such as graphene and graphene oxide (GO), introduced ultrathin membranes with exceptionally high gas permeability while maintaining precise molecular sieving capabilities [6–8]. Additionally, carbon nanotube (CNT) membranes have exhibited near-frictionless gas transport, enabling ultrafast diffusion rates while maintaining strong selectivity [9].

Beyond these fundamental advancements, hybrid and composite membranes integrating carbon materials with polymers and metal-organic frameworks (MOFs) have enhanced mechanical stability and separation efficiency [10]. Meanwhile, microporous carbon membranes tailored for $CO_2$ capture have demonstrated superior selectivity and permeability, offering a viable approach for mitigating industrial emissions [11]. More recently, research has focused on improving the scalability, durability, and cost-effectiveness of carbon-based membranes, addressing challenges related to fabrication and industrial integration. Among these, graphynes, a family of two-dimensional (2D) carbon materials featuring sp- and $sp^2$-hybridized carbon atoms, have attracted increasing attention due to their unique structural and electronic characteristics [12, 13]. Unlike graphene, which consists entirely of $sp^2$-hybridized carbon atoms, graphynes incorporate acetylenic linkages between benzene rings, resulting in a tunable band gap, intrinsic porosity, and anisotropic transport properties. These features make graphynes highly promising for applications in gas separation, catalysis, and nanoelectronics [14, 15].

Theoretical studies have predicted various graphyne allotropes, including α-, β-, γ-, and 6,6,12-graphyne, each with distinct lattice structures and electronic behaviors [16]. Computational simulations suggest that these materials exhibit superior gas selectivity, particularly for hydrogen and carbon dioxide, due to their well-defined nanopores [17]. Additionally, their intrinsic semiconducting nature and high carrier mobility position them as candidates for next-generation electronic and optoelectronic devices [18]. Despite their promising properties, the experimental realization of graphynes remains a significant challenge due to the difficulty in achieving large-scale synthesis with precise structural control.

To date, graphdiyne [13], a closely related structure containing diacetylenic linkages, has been successfully synthesized and demonstrated exceptional chemical stability, high porosity, and strong adsorption capabilities [19]. This breakthrough has paved the way for experimental investigations into the gas separation, energy storage, and catalytic properties of sp–$sp^2$ hybridized carbon materials. However, the synthesis of pure graphyne structures beyond graphdiyne remains an ongoing challenge, with research efforts focused on templated growth, catalytic coupling reactions, and bottom-up organic synthesis strategies.

Recent theoretical studies have shown that mono and multilayer graphtriyne membranes exhibit high hydrogen permeability [20], making them promising candidates for hydrogen purification and energy storage applications. Computational simulations have confirmed that their sub-nanometer pores allow selective $H_2$ diffusion, while effectively blocking larger gas molecules like $CO_2$, $N_2$ and $H_2O$ [21]. Furthermore, graphtriyne has shown a strong affinity for $CO_2$ adsorption, followed by $H_2O$ and $N_2$ [22, 23]. These studies have also hypothesized that the binding energy order can be broadly explained by the relative electric dipole moments and polarizabilities of the different gases [21]. Beyond the qualitative nature of these conclusions, key aspects of intermolecular forces—such as the role of Pauli repulsion, which includes spin repulsion and intermolecular electron exchange, as well as multipolar electrostatic interactions—may significantly influence the interaction between these gases and the membrane. This study investigates the role of these factors, along with dispersion and inductive phenomena, in the adsorption of $CO_2$, $N_2$, and $H_2O$ by graphtriyne membranes through interaction energy decomposition analysis. The results presented here are preliminary, based on static calculations. As a next step they must be validated against those obtained from dynamic simulations, which enable a more comprehensive exploration of the configurational space and incorporate thermal effects into the analysis.

## 2 Methodology

In this study, we investigated the adsorption of three gases, $CO_2$, $N_2$, and $H_2O$, using monolayer and trilayer graphtriyne membranes. The adsorption pores of these membranes were simulated based on molecular models depicted in Fig. 1, which are consistent with those used in previous studies. The geometrical parameters of both the membrane models and gas molecules were kept fixed throughout the calculations, with the most relevant parameters also presented in the figure. Regarding the monolayer and trilayer models: each layer is represented by a octadecadehydrotribenzo annulene molecule with $D_3h$ symmetry and the C-C and C-H distances shown in Fig. 1, which corresponds to those previously obtained from DFT periodic calculations [20, 21]. In the trilayer model, the interlayer distance is 3.45 Å, and the layers are intercalated with a displacement of 1.6 Å between the geometric centers of the inner and outer layers (parameters also illustrated in Fig. 1).

The calculations were performed at the Density Functional Theory (DFT) level using the M06-2X functional combined with the 6-311++G(2df,pd) basis set. This functional was shown to be suitable to investigate non-covalent interactions [24] and has been shown to accurately capture most of the dispersion energy in complexes involving carbon allotropes, including graphene, when compared to other functionals [25]. The basis set employed is sufficiently large to ensure an accurate representation of the electron polarization. Explicit D3 dispersion corrections, as developed by Grimme et al. [26], were also included in the calculations. Interaction energies were computed using the supermolecule approach and further decomposed into electrostatic, Pauli repulsion, and polarization contributions via Deformation Density-based Energy Decomposition Analysis (DD-EDA) [25, 27]. To account for Basis Set Superposition Error (BSSE), all energies were corrected using the counterpoise method of Boys and Bernardi [28].

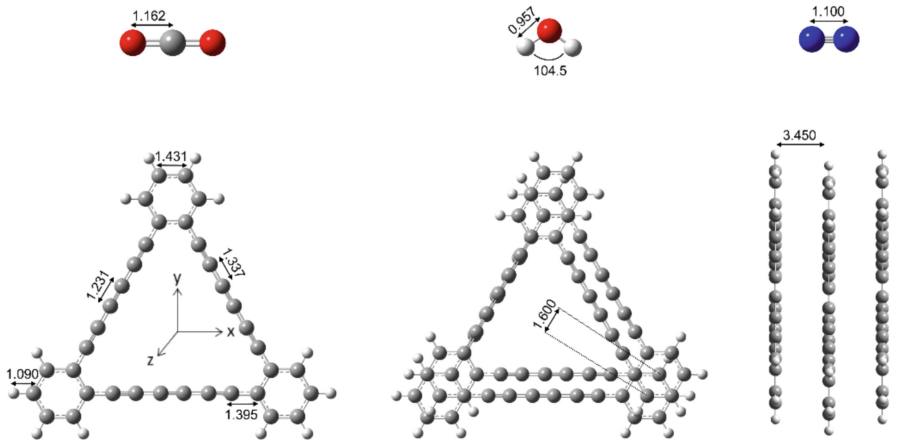


**Fig. 1.** Main geometrical parameters of the molecules, monolayer and trilayer models of the graphtriyne membranes. Distances in Angstroms and angles in degrees.

Electron densities were calculated with the Gaussian 16 software package [29], and the DD-EDA was performed with the EDA-NCI program [30].

The Pauli repulsion energy was further decomposed into its attractive component (intermolecular exchange) and its repulsive component (spin repulsion) using the DD-EDA method. Additionally, the polarization energy was divided into induction and dispersion contributions. However, this decomposition relies on defining molecular fragments within the Hilbert space of the basis functions, requiring the use of basis sets without diffuse functions to ensure reliable results. To address this, calculations were repeated using the 6-311G(d,p) basis set, allowing for a detailed analysis of the dispersion and induction contributions to polarization energy. This smaller basis set also provided a means to assess the influence of polarization and diffuse functions on the computed energy terms.

## 3 Results

### 3.1 Monolayer Membrane

The initial step was to determine the most stable orientation of the molecules within the monolayer membrane pore by calculating the relative strength of the interaction at the pore center. This was followed by a scan along the perpendicular direction to the membrane surface for the most stable orientation, starting from the pore center up to a distance of 3.2 Å. This approach builds upon the previous analysis conducted by Bartolomei et al. [21] but extends it to include the different interaction energy components, providing deeper insight into the adsorption mechanisms and relative stabilities of the molecules within the pore.

The interaction energy values and their components for $CO_2$, $N_2$, and $H_2O$ molecules positioned at the center of the monolayer membrane—with their main symmetry axis aligned along the x, y, or z directions—are presented in Table 1. Figure 1 illustrates

the orientation of the Cartesian axes in the monolayer. As observed, the most stable orientation for $CO_2$ and $N_2$ is with the molecular axis aligned along the z direction, while for $H_2O$, it is with the $C_2$ symmetry axis aligned along the y direction, consistent with the findings of Bartolomei et al. [21]. The EDA analysis reveals that the destabilization in the other two orientations in $CO_2$ and $N_2$ is primarily due to a significant increase in spin repulsion energy, which is not offset by corresponding increases (in negative terms) in electrostatic, polarization, and intermolecular exchange energies. Given the well-known relationship between Pauli energy and steric hindrance, this suggests that these molecules orient themselves within the membrane pore to minimize steric interactions as much as possible. In contrast, for $H_2O$, the most favorable orientation is the one with greater (more negative) electrostatic, polarization, and intermolecular exchange energies, which compensate for the increased spin repulsion.

**Table 1.** Total interaction energy and its different components for the interaction of the monolayer membrane with $CO_2$, $N_2$, and $H_2O$ positioned at the center of the monolayer membrane and oriented with their main symmetry axis aligned along the x, y, or z directions (see Fig. 1). Elec, Exch, Rep, Pol and Tot, refer to electrostatic, intermolecular exchange, spin repulsion, polarization and total energies, respectively. Atrac is the summation of all attractive energy terms, namely, Elec, Exch and Pol.

| | Elec | Exch | Rep | Pol | Atrac | Tot |
|---|---|---|---|---|---|---|
| **$CO_2$** | | | | | | |
| **X**[a] | −11.07 | −40.53 | 76.16 | −12.03 | −63.63 | 12.53 |
| **Y**[a] | −12.29 | −41.38 | 80.19 | −12.28 | −65.95 | 14.24 |
| **Z** | −2.09 | −7.14 | 10.74 | −5.13 | −14.36 | −3.61 |
| **$N_2$** | | | | | | |
| **X**[a] | −1.67 | −9.46 | 15.88 | −2.86 | −14.00 | 1.87 |
| **Y**[a] | −1.67 | −9.50 | 16.02 | −2.82 | −13.99 | 2.03 |
| **Z** | −1.68 | −8.47 | 13.04 | −4.92 | −15.07 | −2.03 |
| **$H_2O$** | | | | | | |
| **X**[a] | 0.50 | 1.49 | −2.54 | 0.64 | 2.63 | 0.09 |
| **Y** | −2.15 | −10.98 | 16.61 | −6.07 | −19.20 | −2.60 |
| **Z**[a] | 1.02 | 2.47 | −4.41 | 1.83 | 5.33 | 0.92 |

[a] These are less stable orientations and their energies are given relative to the most stable one.

Figure 2 compares the interaction energy and its components as the molecules are moved along the perpendicular direction to the membrane plane. $CO_2$ exhibits the most favorable adsorption, as its interaction energy remains more negative than that of the other two molecules throughout the scan. However, in the 1.2–1.8 Å range, its values are very close to those of $H_2O$. At the limiting distance of 3.2 Å considered in this study, the interaction energies of all three molecules converge, with $H_2O$ and $N_2$ showing nearly identical values.

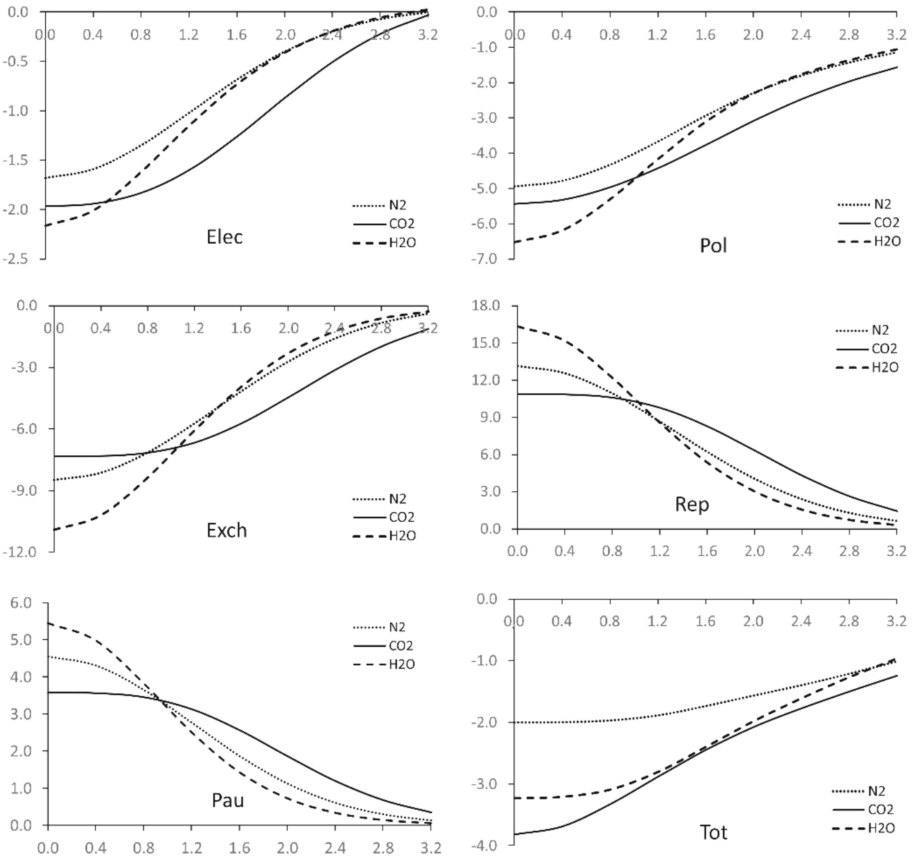


**Fig. 2.** Electrostatic (Elec), polarization (Pol), intermolecular exchange (Exch), spin repulsion (Rep), Pauli (Pau) and total (Tot) interaction energies vs the distance between the geometrical center of the molecule and that of the monolayer membrane in the perpendicular detachment of the adsorption complex. Energies were obtained with the 6-311++G(2df,pd) basis set and are expressed in kcal/mol, distances are expressed in Angstroms.

The behavior of the interaction energy components is somewhat unexpected, as their contributions to the relative stability of the complexes change along the scan. At short distances from the membrane center, $CO_2$'s greater stability arises from its lower spin repulsion energy, even though the attractive terms are consistently stronger for $H_2O$, and even for $N_2$ in the case of intermolecular exchange. However, beyond 1.0 Å, spin repulsion increasingly destabilizes $CO_2$ relative to $H_2O$ and $N_2$. This destabilization is counterbalanced by attractive forces, which become more negative for $CO_2$ beyond 0.6 Å, 1.0 Å, and 1.1 Å for electrostatic, polarization, and intermolecular exchange energies, respectively. These findings suggest that $CO_2$ adsorption is initially driven by the attractive intermolecular forces but, at closer distances, is stabilized by a reduction in repulsion forces.

An unexpected result is that $H_2O$ exhibits a larger (more negative) polarization energy than $CO_2$ and $N_2$ at distances below 1.0 Å, despite having only one heavy atom, compared to three in $CO_2$ and two in $N_2$. Given $H_2O$'s lower overall polarizability, a lower polarization energy would typically be expected. This anomaly is explained by the orientation of $H_2O$ within the pore, with its most polarizable atom, oxygen, positioned at the center. In contrast, $CO_2$ has its carbon atom at the center, with oxygen atoms positioned at a distance of 0.957 Å, while $N_2$ has no central atom, with each nitrogen positioned 0.55 Å away. As the molecules move perpendicularly to the membrane, the oxygen atom in $H_2O$ shifts away from the center while one of $CO_2$'s oxygen atoms moves closer, reversing the polarization energy trend between these two molecules.

Figure 3 further decomposes the polarization energy into induction and dispersion terms using a basis set that excludes diffuse functions, as described in the methodology. The polarization energy scan closely resembles the one obtained with the basis set including diffuse functions, suggesting that the partitioning into induction and dispersion can be reasonably extrapolated to the larger basis set.

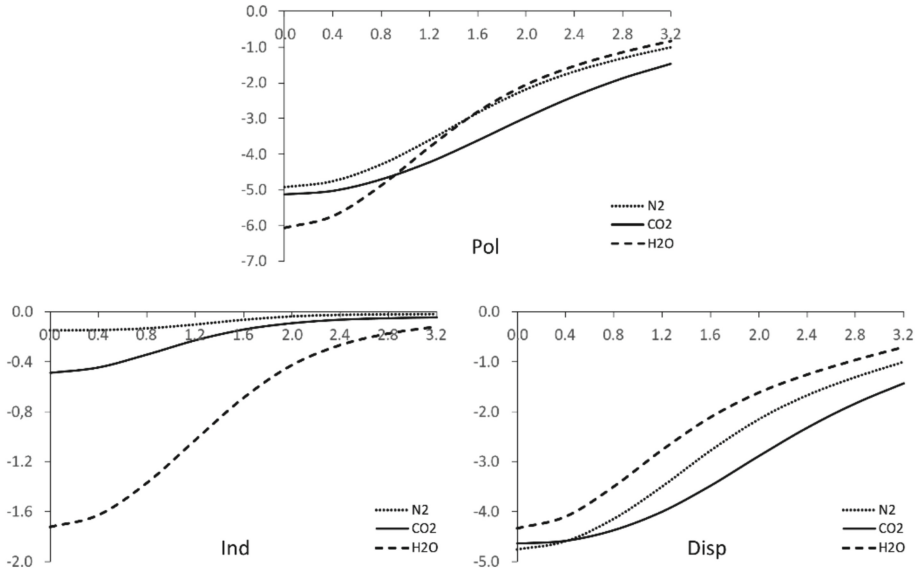


**Fig. 3.** Polarization (Pol), induction (Ind) and dispersion (Disp) energies vs the distance between the geometrical center of the molecule and that of the monolayer membrane in the perpendicular detachment of the adsorption complex. Energies were obtained with the 6-311G(d,p) basis set and are expressed in kcal/mol, distances are expressed in Angstroms.

From the induction energy scan, we observe that $H_2O$ consistently exhibits the most negative induction energy, as expected due to its large dipole moment and its orientation relative to the membrane plane. $CO_2$ follows, as it has bond dipole moments but is oriented perpendicularly to the membrane plane. Lastly, $N_2$ shows a negligible induction energy due to the nonpolar nature of its single bond.

Regarding the dispersion term, $CO_2$ and $N_2$ exhibit more negative values than $H_2O$ throughout the scan. When positioned near the center of the membrane, $CO_2$ and $N_2$ have nearly identical dispersion energies. However, at larger distances, $CO_2$ shows a more negative dispersion energy than $N_2$.

The relative stability order of $CO_2 > H_2O > N_2$ can be also qualitatively understood by examining the spin repulsion and polarization densities, which correspond to the Pauli and polarization energies, respectively. Figure 4 compares the spin repulsion and polarization densities at the center of the membrane pore for the three molecules. As shown in the figure, spin repulsion exhibits negative values, representing electron depletion, in the intermolecular region due to the overlap between the electron clouds of the molecule and the membrane. Conversely, positive values, representing electron accumulation, are observed near the atoms of both the molecule and the membrane. The negative regions are slightly more pronounced in $H_2O$, followed by $N_2$ and then $CO_2$, aligning with the Pauli and spin repulsion energy trends shown in Fig. 2 at short distances from the membrane center.

The polarization densities shown in Fig. 4 reveal distinct characteristics for $CO_2$, $N_2$, and $H_2O$. In $CO_2$ and $N_2$, the polarization densities reflect the typical behavior of highly dispersive interactions, with electron density migrating from the molecules to the intermolecular region. In $H_2O$, induced dipoles are also observed along the molecular skeleton of the membrane and within the O-H bonds, highlighting the significant contribution of induction interactions. The magnitude of polarization density follows the trend: $N_2 < CO_2 < H_2O$, aligning with the order of polarization energies obtained at the center of the membrane.

Regarding the total densities, which result from the superposition of spin repulsion and polarization, it is observed that for the most stable complexes—$CO_2$ and $H_2O$—the total deformation density more closely resembles the polarization component than the spin repulsion. In contrast, for $N_2$, the total deformation density aligns more closely with the spin repulsion, which qualitatively accounts for the lower stability of this complex.

### 3.2 Trilayer Membrane

The next step in our analysis was to construct a trilayer membrane (see Fig. 1), following the same procedure as Bartolomei et al. [20, 21], and perform a DD-EDA of the interaction energy for $CO_2$, $N_2$, and $H_2O$ at the three most relevant positions within the membrane: the center of the inner layer, the center of the interlayer region, and the center of one of the outer layers. These positions are illustrated in Fig. 5 for the $N_2$ molecule. For consistency, the most stable orientation of each molecule in the monolayer membrane was used in the trilayer study.

Table 2 presents the results obtained for the interaction energy and its main components, calculated using the 6-311++G(2df,pd) and 6-311G(d,p) basis sets. The total interaction energy differences between these basis sets are negligible in the case of $N_2$, more significant in $CO_2$, and relevant in $H_2O$, with maximum deviations of 2.3%, 9.7% and 20.4%, respectively. However, differences in polarization energies are smaller, with maximum deviations of 2.4%, 4.9% and 9.0%. It should be noted that the larger basis set produces more negative interaction energies in all cases.

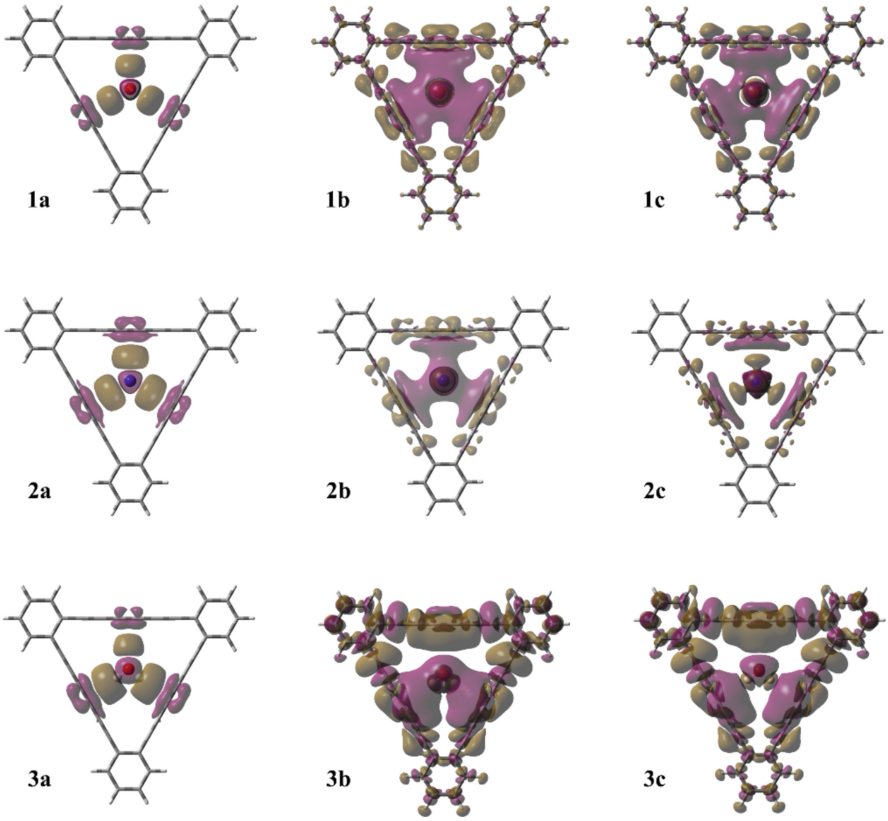


**Fig. 4.** Spin repulsion (**a**), polarization (**b**) and total deformation (**c**) densities arising from the interaction of $CO_2$ (**1**), $N_2$ (**2**) and $H_2O$ (**3**) molecules with a monolayer membrane of graphtriyne. In all cases, the complex corresponds to the lowest energy conformation. Brown and magenta colors represent electron density depletion and accumulation, respectively. Plots were represented with an isosurface value of $5{\cdot}10^{-4}$ Densities were obtained with the 6-311++G(2df,pd) basis set.

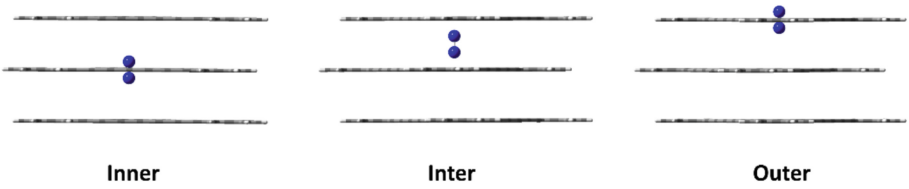


**Fig. 5.** Positions selected within the trilayer membrane model for the N2 molecule. These are same positions selected for $CO_2$ and $H_2O$.

Given that a basis set without diffuse functions is required to decompose polarization into induction and dispersion, and that the differences in polarization energy remain below 9.0%, we will use the larger basis set to analyze all energy components except induction and dispersion, for which the smaller basis set will be employed.

**Table 2.** Total interaction energy and its different components for the interaction of the trilayer membrane of graphtriyne with a $CO_2$, $N_2$ and $H_2O$ molecule located at the geometric center of the inner layer, the outer layer and between the inner and an outer layers. All energies in kcal/mol.

| | Inner[a] | Inter[a] | Outer[a] | Inner[b] | Inter[b] | Outer[b] |
|---|---|---|---|---|---|---|
| **$CO_2$** | | | | | | |
| **Elec** | −2.51 | −4.76 | −2.14 | −2.57 | −4.85 | −2.21 |
| **Pau** | 6.83 | 13.01 | 5.21 | 6.81 | 13.04 | 5.21 |
| Exch | −14.33 | −21.24 | −10.85 | −14.05 | −21.19 | −10.62 |
| Rep | 21.17 | 34.25 | 16.06 | 20.87 | 34.23 | 15.84 |
| **Pol** | −10.20 | −11.35 | −7.92 | −9.70 | −10.99 | −7.54 |
| Ind | −4.19 | −3.67 | −2.69 | −0.75 | −0.70 | −0.61 |
| Disp | −6.02 | −7.68 | −5.23 | −8.96 | −10.29 | −6.93 |
| **Tot** | −5.88 | −3.10 | −4.85 | −5.46 | −2.80 | −4.53 |
| **$N_2$** | | | | | | |
| **Elec** | −1.73 | −2.54 | −1.63 | −1.77 | −2.61 | −1.68 |
| **Pau** | 5.42 | 8.12 | 4.98 | 5.42 | 8.05 | 4.99 |
| Exch | −10.97 | −14.30 | −9.77 | −10.81 | −14.08 | −9.64 |
| Rep | 16.38 | 22.42 | 14.75 | 16.23 | 22.13 | 14.63 |
| **Pol** | −7.55 | −8.45 | −6.31 | −7.43 | −8.25 | −6.25 |
| Ind | −0.61 | 0.14 | −0.03 | −0.23 | −0.48 | −0.20 |
| Disp | −6.94 | −8.59 | −6.28 | −7.20 | −7.78 | −6.05 |
| **Tot** | −3.86 | −2.87 | −2.96 | −3.77 | −2.81 | −2.94 |
| **$H_2O$** | | | | | | |
| **Elec** | −1.87 | −2.15 | −1.95 | −1.86 | −2.13 | −1.94 |
| **Pau** | 5.67 | 6.01 | 5.54 | 5.82 | 6.12 | 5.71 |
| Exch | −11.92 | −12.46 | −11.40 | −11.72 | −12.25 | −11.33 |
| Rep | 17.59 | 18.47 | 16.94 | 17.53 | 18.37 | 17.04 |
| **Pol** | −8.31 | −8.08 | −7.45 | −7.56 | −7.39 | −6.86 |
| Ind | −2.39 | −2.19 | −1.95 | −1.76 | −1.44 | −1.72 |
| Disp | −5.92 | −5.89 | −5.50 | −5.80 | −5.95 | −5.13 |
| **Tot** | −4.52 | −4.22 | −3.86 | −3.60 | −3.40 | −3.09 |

[a] Values calculated with the 6-311++(2df,pd) basis set.
[b] Values calculated with the 6-311(d,p) basis set.

Based on the data in Table 2, it can be concluded that **$CO_2$** is the most stabilized molecule at the center of both the inner and outer layers, while $H_2O$ is more stabilized at the interlayer position. As observed in the monolayer case, **$N_2$** is the least stabilized molecule within the trilayer membrane. Unlike the monolayer case, the greater stability

of $\mathbf{CO_2}$ at the center of a layer (either inner or outer) in the trilayer membrane results from more negative values of all attractive terms, with the most significant contributions coming from intermolecular exchange and dispersion energies. In contrast, the spin repulsion for $\mathbf{CO_2}$ is larger than that for $\mathbf{N_2}$ and $\mathbf{H_2O}$. These differences, compared to the monolayer case—where the largest stabilization of $CO_2$ is attributed to a decrease in spin repulsion—highlight the significant impact of interactions with neighboring layers in a multilayer membrane.

The greater stability of $H_2O$ at the center of the interlayer region results from a significant increase in spin repulsion energy for $CO_2$, and to a lesser extent for $N_2$, which is not compensated by the attractive terms. As a result, $CO_2$ experiences a notable decrease in stability from the center of the inner and outer layers to the interlayer region, suggesting that the orientation of these molecules may not be optimal in the interlayer region. This points to the need for a more thorough exploration of the potential energy surface, along with a dynamic study, as mentioned at the end of the Introduction section. In contrast, the stability of $H_2O$ remains relatively stable along the trilayer, with a slight increase as the molecule penetrates deeper into the membrane.

The results obtained for $CO_2$ differ from those reported in Reference 21 for the total interaction energies, where the value at the center of the interlayer region is nearly identical to that at the center of the inner layer. This discrepancy may stem from the different computational approaches used, DFT-D3 in this study and MP2C in Reference 21. However, the exact cause remains unclear and could be attributed to an underestimation of spin repulsion in the interlayer region at the MP2C level, an underestimation of dispersion energy at the DFT-D3 level, or even the use of the counterpoise correction in Reference 21. In principle, the counterpoise correction is not recommended for post-SCF methods involving multi determinant wave functions, unless it is used in conjunction with a complete basis set extrapolation scheme [31]. This will be particularly relevant for large systems like the trilayer membrane model. Further investigation is needed to clarify the differences observed between these computational approaches.

Finally, it is important to highlight the effect of diffuse functions on the decomposition of polarization into induction and dispersion terms. In $CO_2$, the largest molecule, there is a clear overestimation of the induction energy, a smaller overestimation in $H_2O$, and no discernible trend in $N_2$. This overestimation occurs due to the extensive penetration of diffuse functions, located on atoms of one molecule, into the spatial regions of nearby atoms in the other molecule. A potential solution would be to perform a real-space partition of the molecular domains instead of a Hilbert space partition, though this approach is computationally more expensive and could be impractical for very large molecular systems.

## 4 Conclusions

In this preliminary study, we explored the differences previously observed in the adsorption affinities of graphtriyne membranes for $CO_2$, $N_2$, and $H_2O$ gas molecules. Analyzing the main components of the interaction energy by means of DD-EDA, we characterized the intermolecular forces governing the relative stability of these molecules when interacting with both monolayer and trilayer membranes.

Our findings indicate that spin repulsion plays a crucial role in the greater stability of $CO_2$ near the pore center of a monolayer membrane. In contrast, during the initial stages of the adsorption process, the attractive terms—electrostatics, intermolecular exchange, and polarization—primarily dictate the relative stability of the different gases.

For interactions with a trilayer membrane, $CO_2$ remains the most stabilized molecule, primarily due to stronger attraction by the different layers, despite experiencing greater spin repulsion compared to the other two gases. The stability order follows the same trend as in the monolayer membrane: $CO_2 > H_2O > N_2$.

**Acknowledgments.** M This work has been funded by the European Union—Next Generation EU under the Italian Ministry of University and Research (MUR) National Innovation Ecosystem grant ECS00000041 - VITALITY - CUP J97G22000170005. N.F.L acknowledges funding by the Italian Ministry of Environment and Energy Security in the framework of the Project GoPV (CSEAA_00011) for Research on the Electric System. M.M.A. thanks Ministerio de Ciencia e Innovación for financial support through the project PID2022-138023NB-I00 and Xunta de Galicia for financial support through the project GRC2024/27.

**Disclosure of Interests.** The authors have no competing interests to declare that are relevant to the content of this article.

## References

1. Baker, R.W., Lokhandwala, K.: Natural gas processing with membranes: an overview. Ind. Eng. Chem. Res. **47**, 2109–2121 (2008)
2. Bernardo, P., Drioli, E., Golemme, G.: Membrane gas separation: a review/state of the art. Ind. Eng. Chem. Res. **48**, 4638–4663 (2009)
3. Hou, R., Fong, C., Freeman, B.D., Hill, M.R., Xie, Z.: Current status and advances in membrane technology for carbon capture. Sep. Purif. Technol. **300**, 121863 (2022)
4. Genduso, G., Ogieglo, W., Wang, Y., Pinnau, I.: Carbon molecular sieve gas separation materials and membranes: a comprehensive review. J. Membr. Sci. **699**, 122533 (2024)
5. Liu, Z., Qiu, W., Quan, W., Koros, W.J.: Advanced carbon molecular sieve membranes derived from molecularly engineered cross-linkable copolyimide for gas separations. Nat. Mat. **22**, 109–116 (2023)
6. Bunch, J.S., Verbridge, S.S., Alden, J.S., van der Zande, A.M., Parpia, J.M., Craighead, H.G., McEuen, P.L.: Impermeable atomic membranes from graphene sheets. Nano Lett. **8**, 2458–2462 (2008)
7. Koenig, S.P., Wang, L., Pellegrino, J., Bunch, J.S.: Selective molecular sieving through porous graphene. Nat. Nanotechnol. **7**, 728–732 (2012)
8. Chumakova, N., Kokorin, A.: Graphene oxide membranes—synthesis, properties, and applications. Mambranes. **13**, 771 (2023)
9. Yazid, A.F., Mukhtar, H., Nasir, R., Mohshim, D.F.: Incorporating carbon nanotubes in nanocomposite mixed-matrix membranes for gas separation: a review. Membranes. **12**, 589 (2022)

10. Dassouki, K., Dasgupta, S., Eddy Dumas, E., Steunou, N.: Interfacing metal organic frameworks with polymers or carbon-based materials: from simple to hierarchical porous and nanostructured composites. Chem. Sci. **14**, 12898–12925 (2023)
11. Lei, L., Bai, L., Lindbråthen, A., Pan, F., Zhang, X., He, X.: Carbon membranes for $CO_2$ removal: status and perspectives from materials to processes. Chem. Eng. J. **401**, 126084 (2020)
12. Malko, D., Neiss, C., Viñes, F., Görling, A.: Competition for graphene: Graphynes with direction-dependent Dirac cones. Phys. Rev. Lett. **108**, 086804 (2012)
13. Li, Y., Xu, L., Liu, H., Li, Y.: Graphdiyne and graphyne: from theoretical predictions to practical construction. Chem. Soc. Rev. **43**, 2572–2586 (2014)
14. Cranford, S.W., Buehler, M.J.: Selective hydrogen purification through graphyne membranes: theory meets experiment. Nanoscale. **4**, 4587–4593 (2012)
15. Qian, X., Li, Y., Li, Y.: Graphyne-based membranes for gas separation. ACS Nano. **12**, 11836–11844 (2018)
16. Perkgoz, N.K., Sevik, C.: Vibrational and thermodynamic properties of α-, β-, γ-, and 6, 6, 12-graphyne structures. Nanotechnology. **25**, 185701 (2014)
17. Azizi, K., Allaei, S.M.V., Fathizadeh, A., Sadeghi, A., Sahimi, M.: Graphyne-3: a highly efficient candidate for separation of small gas molecules from gaseous mixtures. Sci. Rep. **11**, 16325 (2021)
18. Majidi, R.: Irida-graphyne: a promising material for optoelectronic applications. Mater. Today Commun. **38**, 107641 (2024)
19. Li, S., Zhao, Y., Wang, D.: Progress in graphdiyne-based membrane for gas separation and water purification. ChemPhysMater. (2025). https://doi.org/10.1016/j.chphma.2025.02.007
20. Bartolomei, M., Carmona-Novillo, E., Giorgi, G.: First principles investigation of hydrogen physical adsorption on graphynes' layers. Carbon. **95**, 1076–1081 (2015)
21. Bartolomei, M., Giorgi, G.: A novel Nanoporous graphite based on graphynes: first-principles structure and carbon dioxide preferential physisorption. ACS Appl. Mater. Interfaces. **8**, 27996–28003 (2016)
22. Apriliyanto, Y.B., Faginas-Lago, N., Lombardi, A., Evangelisti, S., Bartolomei, M., Leininger, T., Pirani, F.: Nanostructure selectivity for molecular adsorption and separation: the case of graphyne layers. J. Phys. Chem. C. **122**, 16195–16208 (2018)
23. Apriliyanto, Y.B., Faginas-Lago, N., Evangelisti, S., Bartolomei, M., Leininger, T., Pirani, F., Pacifici, L., Lombardi, A.: Multilayer graphtriyne membranes for separation and storage of CO2: molecular dynamics simulations of post-combustion model mixtures. Molecules. **27**, 5958 (2022)
24. Zhao, Y., Truhlar, D.G.: The M06 suite of density functionals for main group thermochemistry, thermochemical kinetics, noncovalent interactions, excited states, and transition elements: two new functionals and systematic testing of four M06-class functionals and 12 other functionals. Theor. Chem. Account. **120**, 215–241 (2008)
25. Ramos-Berdullas, N., Pérez-Juste, I., Van Alsenoy, C., Mandado, M.: Theoretical study of the adsorption of aromatic units on carbon allotropes including explicit (empirical) DFT dispersion corrections and implicitly dispersion-corrected functionals: the pyridine case. Phys. Chem. Chem. Phys. **17**, 575–587 (2015)
26. Grimme, S., Antony, J., Ehrlich, S., Krieg, H.: A consistent and accurate ab initio parametrization of density functional dispersion correction (DFT-D) for the 94 elements H-Pu. J. Chem. Phys. **132**, 154104 (2010)
27. Mandado, M., Hermida-Ramón, J.M.: Electron density based partitioning scheme of interaction energies. J. Chem. Theory Comput. **7**, 633–641 (2011)
28. Boys, S.F., Bernardi, F.: The calculation of small molecular interactions by the differences of separate total energies. Some procedures with reduced errors. Mol. Phys. **19**, 553–566 (1970)

29. Frisch, M.J., et al: Gaussian 16 Revision C.01. (2016)
30. Mandado, M., Van Alsenoy, C.: EDA-NCI: Energy Decomposition Analysis of Non-Cova-lent Interactions. https://github.com/marcos-mandado/EDA-NCI, last accessed 27 March 2025
31. Halkier, A., Klopper, W., Helgaker, T., Jörgensen, P., Taylor, P.R.: Basis set convergence of the interaction energy of hydrogen-bonded complexes. J. Chem. Phys. **111**, 9157–9167 (1999)